JACS
JOURNAL OF THE AMERICAN CHEMICAL SOCIETY
Article
Cite This: J. Am. Chem. Soc. 2019, 141, 497−504
pubs.acs.org/JACS

Mechanical Deformation Distinguishes Tunneling Pathways in Molecular Junctions

Zuoti Xie,[†] Ioan Bâldea,*[,§] Greg Haugstad,[‡] and C. Daniel Frisbie*[,†]

[†]Department of Chemical Engineering and Materials Science and [‡]Characterization Facility, University of Minnesota, Minneapolis, Minnesota 55455, United States

[§]Theoretische Chemie, Universität Heidelberg, INF 229, D-69120 Heidelberg, Germany

Supporting Information

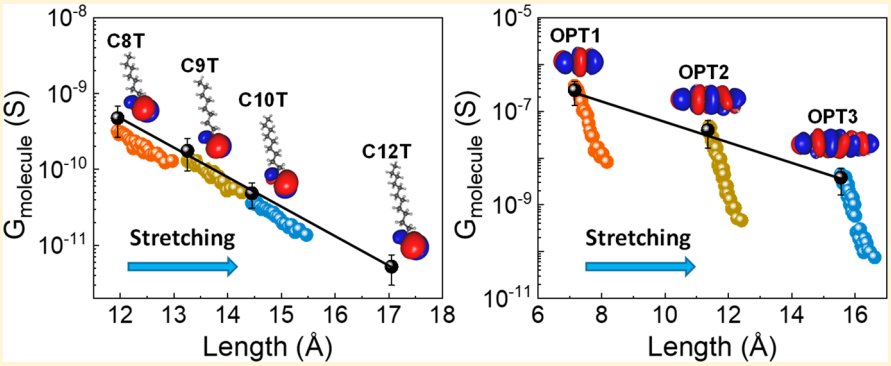

ABSTRACT: Developing a clearer understanding of electron tunneling through molecules is a central challenge in molecular electronics. Here we demonstrate the use of mechanical stretching to distinguish orbital pathways that facilitate tunneling in molecular junctions. Our experiments employ junctions based on self-assembled monolayers (SAMs) of homologous alkanethiols (C*n*T) and oligophenylene thiols (OPT*n*), which serve as prototypical examples of σ-bonded and π-bonded backbones, respectively. Surprisingly, molecular conductances ($G_{molecule}$) for stretched C*n*T SAMs have exactly the same length dependence as unstretched C*n*T SAMs in which molecular length is tuned by the number of CH_2 repeat units, *n*. In contrast, OPT*n* SAMs exhibit a 10-fold-greater decrease in $G_{molecule}$ with molecular length for stretched versus unstretched cases. Experiment and theory show that these divergent results are explained by the dependence of the molecule−electrode electronic coupling Γ on strain and the spatial extent of the principal orbital facilitating tunneling. In particular, differences in the strain sensitivity of Γ versus the repeat-length (*n*) sensitivity can be used to distinguish tunneling via delocalized orbitals versus localized orbitals. Angstrom-level tuning of interelectrode separation thus provides a strategy for examining the relationship between orbital localization or delocalization and electronic coupling in molecular junctions and therefore for distinguishing tunneling pathways.

INTRODUCTION

Advances in molecular electronics depend on achieving a thorough understanding of charge transport mechanisms in the field's most basic construct, the nanoscale metal−molecule−metal junction.[1−10] Identifying which molecular orbitals participate in tunneling transport through molecular junctions is often a central question that can be surprisingly difficult to answer.[9,11−14] The difficulty arises in part because determining the participating orbitals requires knowledge not only of the electronic structure of the component molecules, which can be obtained by quantum chemical methods,[15,16] but also of the orbital energy alignment with respect to the Fermi level of the contacts, which is more difficult to predict quantitatively and also challenging to measure experimentally.[14,17−19] The situation is compounded if there are multiple molecular states relatively close in energy or, in contrast, states well-separated in energy but with vastly different degrees of spatial localization.[7,20−22] The latter case applies to junctions based on the deceptively simple alkanethiols, for example, where both the localized highest occupied molecular orbital (HOMO) and the spatially extended HOMO-1 have been implicated in transport.[12−14,23,24]

Here we show by experiment the clear difference between tunneling assisted by a localized "gateway" orbital,[7,10] with σ character, and a fully delocalized π-conjugated orbital. Our approach involves measurements of the conductance of molecular junctions as a function of mechanical deformation using the well-known conducting probe atomic force microscopy (CP-AFM) platform. Prior work has shown that single-molecule conductance is sensitive to mechanical deformation,[25−31] but a side-by-side comparison of the

Received: October 18, 2018
Published: December 8, 2018

DOI: 10.1021/jacs.8b11248
J. Am. Chem. Soc. 2019, 141, 497−504

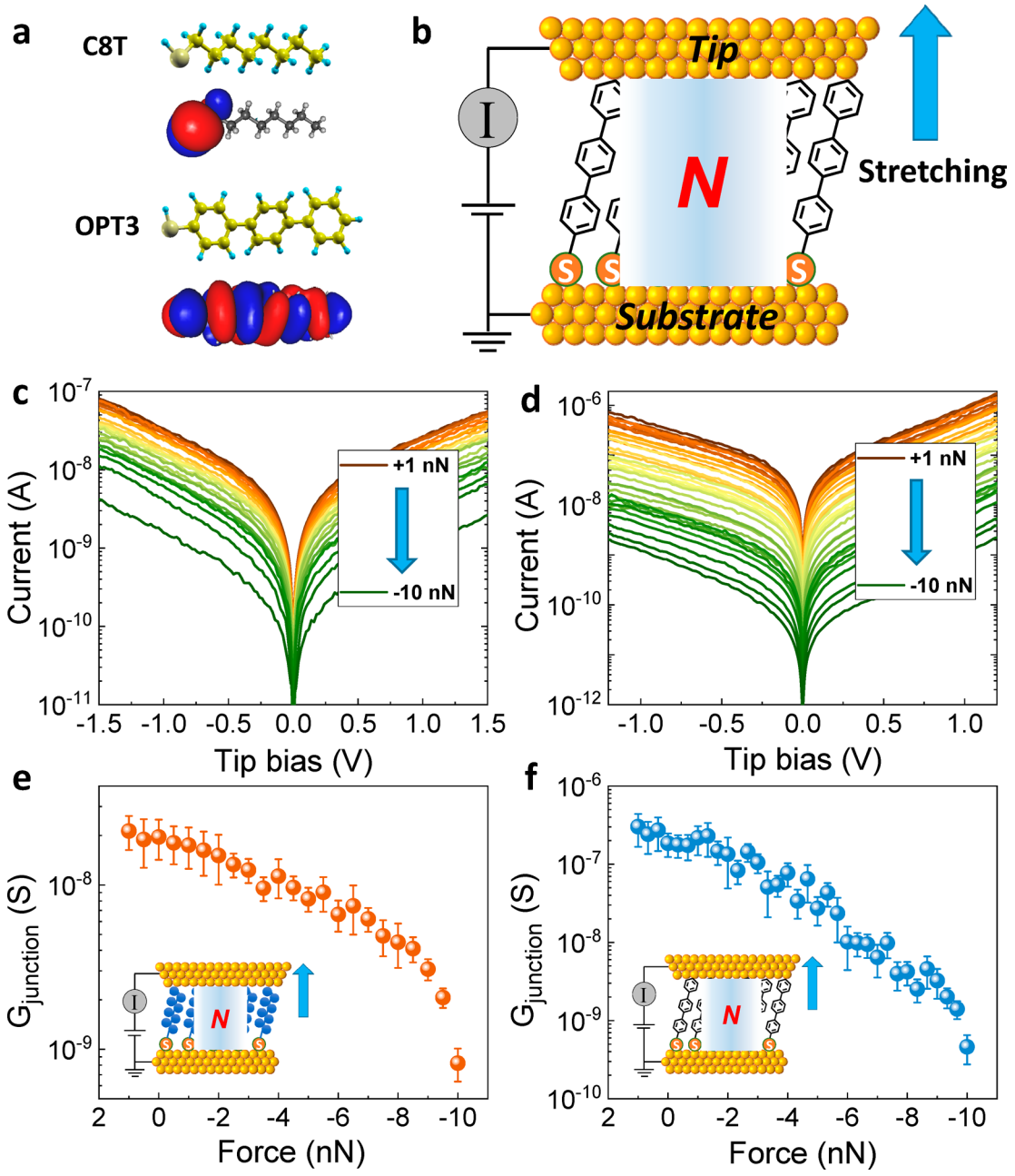

Figure 1. Molecules, experimental setup, and raw transport measurements. (a) Geometries and HOMO distributions for the same molecular orientations of the C8T and OPT3 molecules investigated in this study. The difference between C8T's HOMO spatial distribution, centered on one end of a molecule possessing an aliphatic backbone characterized by electrons localized on C−C σ-bonds and OPT3's HOMO spatial distribution, extending over an aromatic molecule characterized by delocalized π-electrons, is reflected in important differences in transport properties of the corresponding junctions under stretching. (b) Schematic representation of the conducting probe atomic force microscopy setup. (c) Averaged $I-V$ traces measured at systematically varying mechanical forces applied to the AFM tip for C8T junctions and (d) OPT3 junctions. Average low-bias junction conductance as a function of applied force for (e) C8T junctions and (f) OPT3 junctions. The error bars represent one standard deviation.

deformation dependence of conductance for σ-bonded aliphatic and π-bonded aromatic molecules has not been reported previously. We find a striking difference in the two cases, which is unambiguously assignable to differences in the strain sensitivity of the molecule−electrode coupling Γ for tunneling through a localized versus a delocalized orbital. Importantly, in the specific case of alkanethiol-based junctions, our results resolve a disagreement in the literature over which orbitals, namely HOMO or HOMO-1, mediate the tunneling conductance.[20,23] More generally, our findings add a definitive example to the growing body of literature showing that mechanical deformation, in combination with theory, provides a unique approach to deciphering transport mechanisms in molecular junctions.[25−31]

EXPERIMENTAL METHODS

Materials. Gold nuggets (99.999% pure) were purchased from Mowry, Inc. (St. Paul, MN). Evaporation boats and chromium evaporation rods were purchased from R. D. Mathis (Long Beach, CA). Silicon (100) wafers were obtained from WaferNet (San Jose,

DOI: 10.1021/jacs.8b11248
J. Am. Chem. Soc. 2019, 141, 497−504

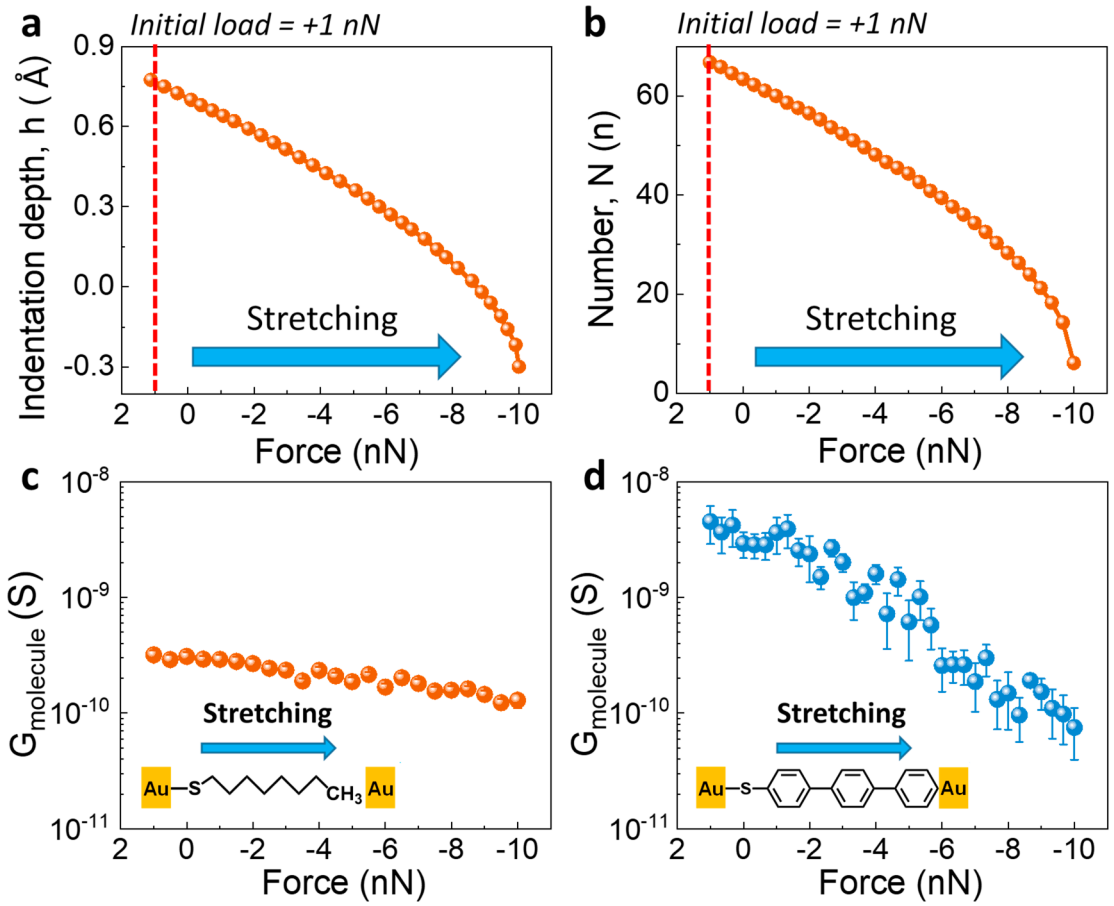

Figure 2. Contact mechanics and low-bias transport data. (a) Indentation depth (h) and (b) number of molecules in the junction (N) vs applied force, computed from the Maugis–Dugdale contact mechanics model. Conductance per molecule vs applied force for (c) C8T junctions and (d) OPT3 junctions based on N as shown in panel b and the conductance data in Figure 1e,f. The error bars represent one standard deviation.

CA). Contact-mode AFM tips (DNP 10 silicon nitride probes) were purchased from Bruker AFM Probes. 1-Octanethiol (C8T) 98.5%, 1-nonanethiol (C9T) 99%, 1-decanethiol (C10T) 99%, 1-dodecanethiol (C12T) 98%, thiophenol (OPT1) 97%, biphenyl-4-thiol (OPT2) 97%, and 1,1′,4′,1″-terphenyl-4-thiol (OPT3) 97% used in this study were purchased from Sigma-Aldrich Company.

Conducting Tip and Sample Preparation. Contact-mode AFM tips were coated with Au at a base pressure of $<10^{-6}$ Torr using a home-built thermal evaporator placed in a N_2-filled glovebox. Films were deposited to a thickness of 500 Å at a rate of 0.5–1.0 Å/s atop a 50 Å Cr adhesion layer. They were immediately transferred without exposure to air to another Ar-filled glovebox housing the CP-AFM to carry out the I–V measurements. The radius of the tip is expected to be ∼50 nm after metal coating.[32] For flat Au substrates, 5000 Å of Au was first deposited onto clean Si wafers in an e-beam evaporator. We then glued Si chips (1 cm × 1 cm) onto the metal surface using epoxy (EPOTEK 377, Epoxy Technologies, MA). The epoxy layer was cured by placing the wafers in an oven at 120 °C for 1 h. The flat Au substrates were peeled off of the silicon surface and immersed in an ethanol solution of molecules at a concentration of ∼1 mM for 20 h. Afterward, the samples were rinsed with ethanol and dried with flowing N_2.

Thickness measurements of the SAMs were carried out with variable-angle spectroscopic ellipsometry (J. A. Woollam Co., Inc.). To do this, measurements of the polarization angles (Ψ and Δ) were recorded as a function of wavelength (λ) from 800 to 1100 nm with 15 nm steps and an incident angle of 65° from the surface normal.

Transport Measurements. CP-AFM-based molecular junctions were fabricated by mounting the substrates in the AFM and bringing the metal-coated tip into contact with the SAM under an ∼+1 nN applied compressive load. With a known spring constant and tuning of the deflection ratio, the variable applied force can be tuned by changing the cantilever deflection set point. Current–voltage measurements were collected at different applied forces. Voltages V were applied to the tip with a Keithley model 236 electrometer operated in DC mode with the sample grounded. Voltage spanned ±1.5 V for CnT junctions and ±1.2 V for OPTn junctions. The slope of the low-bias I–V characteristic (linear portion within the bias range of ±0.1 V) was used to define a junction (low-bias) conductance $G_{junction}$. The tunneling efficiency parameter β could be obtained from the linear fit of the semilog plot of low-bias conductance versus molecule length.

Quantum Mechanical Calculations. The molecular geometries shown in Figures 1a, S4a, S5a, S6, S9a, and S10a generated with XCrysDen[33] were optimized at the DFT/B3LYP/6-311++g(d,p) level by using *Gaussian 09*.[34] HOMO spatial distributions shown in Figures 1a, S4a, S5a, S6, S9a, and S10a generated with GABEDIT[35] were computed with CFOUR[36] as described in ref 37.

RESULTS AND DISCUSSION

CP-AFM molecular junctions based on alkanethiols (CnT, n = 8, 9, 10, 12) and oligophenylene thiols (OPTn, n = 1,2, 3) investigated in this work (Figure 1a), which are known to form good self-assembled monolayers (SAMs) on Au,[38,39] provide an excellent opportunity to examine the impact of a mechanical force on the tunneling transport in both the linear and nonlinear bias ranges. All measurements in conjunction with the present study were completed in an Ar-filled glovebox at room temperature. To establish a stable contact between the tip and the molecules in the CP-AFM molecular junctions

DOI: 10.1021/jacs.8b11248
J. Am. Chem. Soc. 2019, 141, 497–504

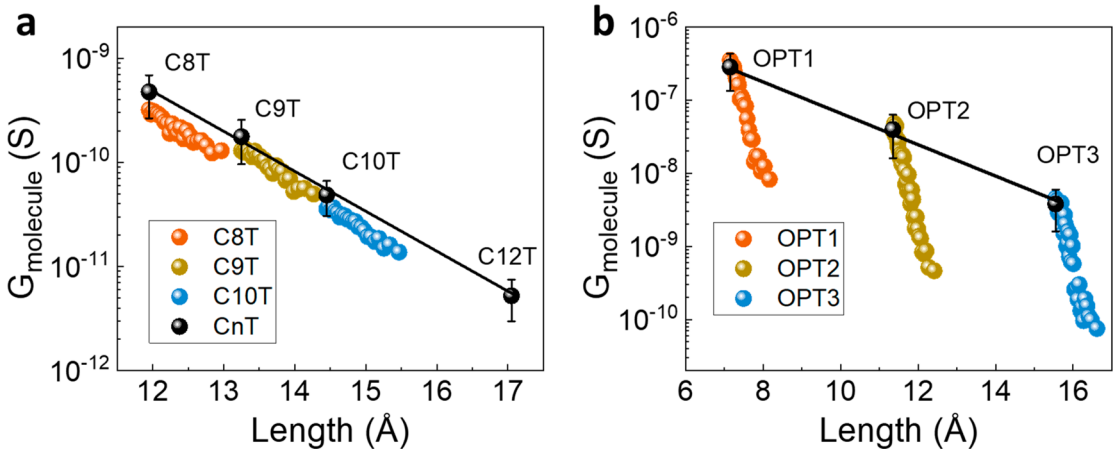

Figure 3. Distinguishing different electron tunneling mechanisms in aliphatic versus aromatic molecules. (a) Length-dependent conductance per molecule for stretched alkanethiol junctions and the corresponding homologous molecular series. Within errors, the conductances of stretched 1-octanethiol (C8T), 1-nonanethiol (C9T), and 1-decanethiol (C10T) junctions exhibit a length dependence similar to that of the nonstretched alkanethiol (C*n*T) series (*n* = 8, 9, 10, and 12). The data provide evidence for medium-assisted tunneling in junctions of alkane monothiols. (b) Length-dependent conductance per molecule for stretched oligophenylene thiol junctions and the corresponding homologous molecular series. Stretched OPT*n*-based junctions (red, yellow, and blue symbols) have conductance varying much more with length than the nonstretched oligophenylene thiol series. The lengths in a and b are the estimated junction lengths, i.e., molecular length corrected by indentation at the corresponding load. The error bars represent one standard deviation.

(Figure 1b), an initial compressive force (F = +1 nN, positive cantilever deflection) was applied to the tip. After the contact was established, the cantilever deflection set point was reduced such that the applied load became increasingly negative (tensile), which increasingly offset the tip−sample adhesive force and thereby reduced the contact compression. At the most negative applied loads (negative cantilever deflection), just prior to the junction breaking, the *net* contact force (applied + adhesive) became tensile rather than compressive (cf. Supporting Information).[32] The value of the rupture or pull-off force (Figure S1, $F \approx -10$ nN on average) was found to be similar for both C*n*T- and for OPT*n*-based SAMs and independent of molecular size *n*.

Figure 1c,d shows averaged $I-V$ traces measured for C8T and OPT3 junctions at different applied forces. In both types of junctions, the current and low-bias conductance were found to decrease with an increasingly tensile applied force. As the force varied from F = +1 nN (applied compressive force) to F = −10 nN (applied tensile force), the conductance of C8T junctions decreased by a factor of ∼20 (Figure 1e) while that of OPT3 junctions decreased by ∼500 times (Figure 1f). Because junctions subject to variable force contain variable numbers of molecules N, the above results cannot be straightforwardly interpreted microscopically; we need to determine properties per molecule not properties per junction. More precisely, we seek the dependence of the conductance per molecule $G_{molecule}$ as a function of molecular length L, as discussed further below.

To estimate the number of molecules per junction $N = N(F)$, which enables us to extract transport properties per molecule, we employed established contact mechanics methods.[40] Calculations using the Maugis−Dugdale (MD) model of contact mechanics[32] (cf. Supporting Information) yielded SAM indentation depths h decreasing from h = 0.8 Å at +1 nN compressive load to h = −0.3 Å at a tensile pull-off force of −10 nN (Figure 2a) and corresponding tip−SAM contact areas decreasing from 19.1 to 1.7 nm^2, respectively (Figure S1b). The contact mechanics results for C*n*T and OPT*n* are very similar, a fact that can be attributed to the similar values of molecular tilt angles (as revealed by our ellipsometry data, Figure S2) and to the similar SAM coverages.[41] Accurate SAM coverages (3.5 molecules/nm^2) were previously determined via Rutherford backscattering spectrometry (RBS) and nuclear reaction analysis (NRA) studies on alkane and oligophenylene thiols.[41] With the values of the force-dependent contact area in hand, we estimated the number of molecules N in the junctions at any F, which was found to decrease from N = 70 to N = 5, corresponding to the junction at initial contact and close to the point of breaking, respectively (Figure 2b). In principle, an opposite F variation, i.e., increasing the compressive force, can yield an increase in the number of molecules in the junction, a process eventually ending with junction damage.

With the numbers of molecules per junction $N = N(F)$ deduced via contact mechanics (Figure 2b), we are able to examine the contributions per molecule to transport properties. With increasing tensile loading, which corresponds to stretching the junction (cf. Supporting Information), the conductance per molecule $G_{molecule}$ for C8T junctions decreased by a factor of ∼2.5 (Figure 2c), which is 20-fold smaller than the factor of ∼50 obtained for OPT3 junctions (Figure 2d). This decrease in conductance upon stretching is consistent with previous studies on single-molecule break junctions based on other molecular species.[26−28]

The decrease in $G_{molecule}$ by a factor of ∼2.5 upon stretching 1-octanethiol (C8T) junctions by ∼0.1 nm (Figure S3a) is a result that appears to be particularly important when it is corroborated with our finding that nonstretched 1-nonanethiol (C9T) junctions have a molecular conductance $G_{molecule}$ that is ∼2.7 times smaller and a length that is 0.12 nm larger than for nonstretched C8T junctions (ellipsometry data, Figure S2). Stimulated by this observation, in Figure 3a we compared the length dependence of $G_{molecule}$ for stretched C8T, C9T, and C10T junctions (obtained by appropriately combining Figure 2a,c with length L = computed molecular length − $h(F)$) with $G_{molecule}$ for the homologous alkanethiol series (C*n*T, *n* = 8, 9,

DOI: 10.1021/jacs.8b11248
J. Am. Chem. Soc. 2019, 141, 497−504

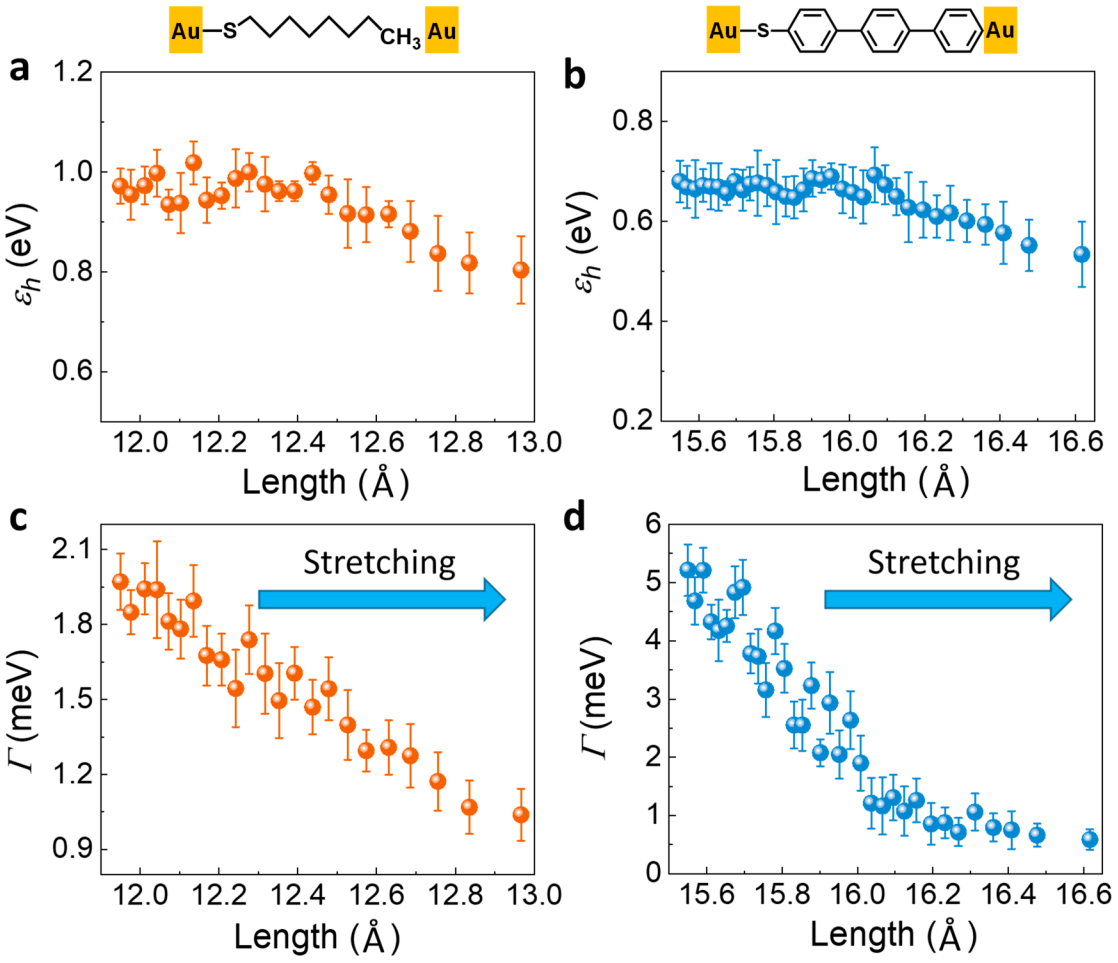

Figure 4. Quantitative results for energy offset and coupling. Average energy offset ε_h and interface coupling Γ versus the junction length for (a, c) C8T and (b, d) OPT3 junctions. ε_h and Γ were obtained by fits of the junction $I-V$ data to an established single-level model of tunneling transport. The error bars represent one standard deviation.

10, 12) under a light compressive applied load, referred to as nonstretched junctions (Figure S3b). The slopes of the data sets in Figure 3a for all stretched junctions (red, yellow, and blue points) are very close to each other, and remarkably, they are essentially identical to the slope for the homologous nonstretched C*n*T series (black points in the same figure; see also the β values of Figures S3a, S3b, S4d, and S5d).

The data in Figure 3a have important implications for understanding transport in alkanethiol junctions. From prior work on the work function dependence of tunneling conductance it is understood that transport is mediated by an occupied orbital. However, both HOMO[42−45] and HOMO-1[23] have been considered, even though these orbitals have very different spatial extensions and are separated in energy by 1.72 eV (C8T) to 1.32 eV (C12T). Quantum chemical calculations[34,36] demonstrate that the C*n*T HOMO is localized on the molecular end chemisorbed on the substrate, as shown in Figure S6a. On binding to Au, the HOMO becomes an Au−S occupied level, also called an interface state in the literature;[46,47] we continue to refer to it as HOMO. By contrast, the HOMO-1 orbital binds C atoms to form the backbone and is extended along the entire molecule, as shown in Figure S6b. The spatial extension of HOMO-1 certainly makes it appear to be an attractive conduit for transport.

Calculations also reveal that the HOMO spatial distribution is practically independent of the number of CH_2 repeat units, and the distribution of the HOMO cloud does not notably change as molecules become stretched; it is only the HOMO distance to the CH_3 end group that changes. In contrast, HOMO-1 is strongly affected by stretching in a manner that is different than simply adding an extra CH_2 repeat unit; electronic clouds between adjacent C−C atoms forming σ bonds become elongated upon stretching, which leads to significant changes in the HOMO-1 energy and electrode−molecule coupling Γ.

Thus, if HOMO-1, which is responsible for C−C σ bonding, yielded a contribution to transport comparable to that of the HOMO, then mechanical stretching would cause dependencies on length that are different from the length dependence of the nonstretched homologous C*n*T series (i.e., slopes of the red, yellow, and blue lines would be different from the slope of the black line in Figure 3a). The clear similarities of the slopes for stretched and unstretched C*n*T molecules eliminate this possibility and are instead consistent with HOMO-only assisted transport. The HOMO, being localized on the sulfur end of the molecule, is not sensitive to stretching. Stretching serves only to increase the distance between the conducting AFM tip and the active orbital (that is, the HOMO) in the same manner as adding a CH_2 group to the backbone, which leads to the remarkable coincidence of the $G_{molecule}$ versus length plots for stretched and unstretched C*n*T molecules. Thus, we find that the stretching experiment provides

DOI: 10.1021/jacs.8b11248
J. Am. Chem. Soc. 2019, 141, 497−504

important qualitative clarification for the tunneling pathway in the C*n*T system.

OPT*n* junctions exhibit very different behavior (Figure 3b). In this case, the dependence of $G_{molecule}$ on length is 10 times steeper for the stretched versus unstretched junctions. This is entirely consistent with the fact that in OPT*n* the HOMO is a π-bonding orbital and delocalized over the molecule (Figure 1a). Deforming the OPT*n* molecules deforms the C−C π-bonds, which leads to changes in the HOMO energy and molecule−electrode coupling Γ and also a strong change in tunneling conductance. We clarify the precise mechanism for the conductance change later below.

For both C*n*T and OPT*n* junctions, the transport mechanism is HOMO-mediated off-resonance tunneling, but it is apparent that there is an important distinction. In an OPT*n* junction, which in a sense is a simpler case, the delocalized HOMO is directly associated with C−C bonding along the entire aromatic backbone, and thus the tunneling mechanism can be aptly referred to as "through-molecule" and "through-bond". For a C*n*T junction, the localized HOMO facilitates tunneling through the molecules, but one might argue that, with respect to the C−C σ-bonded backbone, the mechanism is not through-bond; i.e., the alkane backbone serves as a conduit, but the HOMO-1 responsible for the σ-bonds does not contribute appreciably. If HOMO-1 did contribute, then the dependence of $G_{molecule}$ on stretching would be similar to that of the HOMO-dominated transport of OPT*n*. Instead, the localized HOMO in C*n*T can be considered to be a "gateway state" for through-molecule transport.[7,10] In this case, the molecular backbone serves as a kind of nonresonant electron channel, and the gateway state determines the energy of highest transmission. Certainly the difference in behavior of the two off-resonance mechanisms, the low conductance one dominated by a localized orbital and the high conductance case dominated by a delocalized orbital, is clearly evident in Figure 3a,b, and these might be considered to be two different types of off-resonance tunneling.

For a more quantitative analysis of the changes in conductance upon stretching, we have processed our transport data with a compact single-level model[48,49] (details in Supporting Information). Our analysis indicates that full *I*−*V* measurements beyond the linear bias range on all of the presently investigated junctions can be accurately reproduced within this model (Figure S7). The single-level model allows an estimation of the effective molecule−electrode coupling Γ and HOMO energy offset ε_h relative to the electrodes' Fermi energy. To assist this analysis, we employed transition voltage spectroscopy (TVS).[50] For all junctions studied, we found that the energy offset[51] decreases by at most ∼0.15 eV upon stretching (Figure 4a,b). Interestingly, a decrease in ε_h should afford an *increase* in $G_{molecule}$, thus this small variation cannot be responsible for the substantial decrease in conductance observed. Rather, similar to cases studied earlier,[17,32] we found that changes in the average HOMO coupling Γ to electrodes upon stretching are substantial for both C*n*T and OPT*n*, and these are mainly responsible for the observed changes in conductance in Figure 3. For example, for C8T, coupling decreases by a factor of 2 from 2 to 1 meV over the range of tensile forces, while OPT3 decreases more sharply, i.e., by a factor of 10 from 5 to 0.5 meV (Figure 4c,d). Noting that (i) $G_{molecule} \propto \Gamma^2 = \Gamma_s\Gamma_t$ (cf. eq S3), where the couplings $\Gamma_{s,t}$ (substrate s and tip t) quantify the rates of charge transfer between the HOMO and the electrodes, and (ii) neither stretching nor additional repeat units notably modify the position of the C*n*T localized HOMO density with respect to the substrate, we arrive at the conclusion that the steep falloff depicted in Figures 3a and 4c for C*n*T junctions may be traced back to the exponential decay of Γ_t (respectively, of the HOMO−tip transfer integral $t_t \approx \sqrt{\Gamma_t}$, cf. Supporting Information) with the HOMO−tip distance ($\sim L$), which does not distinguish whether L is increased mechanically (i.e., by stretching) or chemically by adding CH_2 units.

In the case of OPT*n*, product $\Gamma^2 = \Gamma_s\Gamma_t \propto t_s^2 t_t^2$ involves spatial averaging of strongly position-dependent quantities t_s and t_t over the contours of the delocalized HOMO (Figure S6c). This makes the conductance dependence on the molecular length of our stretched OPT*n* junctions much steeper than that characterizing the unstretched OPT*n* series (Figure 3b), indicating a very strong sensitivity of through-π-bond tunneling to tiny changes in π interactions within the phenyl rings. More generally, one can conclude that tunneling through spatially extended orbitals like the HOMO of OPT*n* will be more sensitive to mechanical strain than tunneling through localized orbitals. The reason is that the total orbital elongation is greater for larger orbitals under tension, and this translates to a net larger change in Γ (Figure 4d).

Consideration should be given to the possible role of intermolecular interactions in these stretching experiments, particularly for the case of OPT*n* junctions (i) that show dramatically different conductance behavior for stretching versus chemical extension and (ii) for which the HOMO is extended along the entire molecular length and thus intermolecular effects might be anticipated. It is important to note that the intermolecular separation d for OPT*n* SAMs is ∼5.3 Å based on the molecular coverage ($\Sigma \approx 3.5$ molecules/nm^2 gives $d = 1/\sqrt{\Sigma} \approx 5.3$ Å). This length is substantially longer than the 3.5−3.6 Å intermolecular separation in bulk van der Waals crystals of typical aromatic molecules.[52−55] Furthermore, extensive quantum mechanical calculations on OPT2 SAMs reveal that even at higher coverages of up to 4.6 molecules/nm^2 (d = 4.7 Å) van der Waals interactions are negligible.[56,57]

Indeed, our data are consistent with this picture of weak lateral interactions in the OPT*n* SAMs. Were there significant lateral intermolecular interactions, one would expect to observe different slopes for the $G_{molecule}$ vs L behavior of OPT1, OPT2, and OPT3. One might also expect to see slope changes for a single species (e.g., changing $G_{molecule}$ vs L behavior for OPT3), which we do not. Thus far, our experimental and computational results indicate that the conductance behavior observed in Figure 3b reflects intramolecular stretching rather than changes in lateral intermolecular interactions.

CONCLUSIONS

We have demonstrated here for the first time a direct, side-by-side comparison of the impact of mechanical stretching on the tunneling conductance of a series of saturated and aromatic molecules. The strikingly different strain response can be unambiguously assigned to differences in the strain sensitivity of Γ, which in turn reflects the very different spatial extent of the HOMO orbitals in C*n*T versus OPT*n* SAMs. That is, mechanical stretching has a qualitatively and quantitatively different impact on the junction charge transport depending on whether the molecular orbital that dominates the charge

DOI: 10.1021/jacs.8b11248
J. Am. Chem. Soc. 2019, 141, 497−504

transport is extended over the molecular backbone or strongly localized on one part. Such experiments in combination with theory thus provide a powerful strategy for assessing tunneling pathways via localized or delocalized orbitals and for building a more comprehensive understanding of transport in molecular tunnel junctions.

■ ASSOCIATED CONTENT

Supporting Information

The Supporting Information is available free of charge on the ACS Publications website at DOI: 10.1021/jacs.8b11248.

Experimental and theoretical details and supplementary tables and figures (PDF)

■ AUTHOR INFORMATION

Corresponding Authors

*ioan.baldea@pci.uni-heidelberg.de.
*frisbie@umn.edu.

ORCID

Zuoti Xie: 0000-0002-1828-0122
Ioan Bâldea: 0000-0003-4860-5757
C. Daniel Frisbie: 0000-0002-4735-2228

Notes

The authors declare no competing financial interest.

■ ACKNOWLEDGMENTS

C.D.F. acknowledges financial support from the U.S. National Science Foundation (CHE-1708173). I.B acknowledges financial support from the Deutsche Forschungsgemeinschaft (DFG grant BA 1799/3-1) and partial computational support from the State of Baden-Württemberg and the DFG through grant no. INST 40/467-1 FUGG. Parts of this work were carried out in the Characterization Facility, University of Minnesota, which receives partial support from the NSF through the MRSEC program.

■ REFERENCES

(1) Tao, N. J. Electron Transport in Molecular Junctions. *Nat. Nanotechnol.* **2006**, *1*, 173−181.
(2) Guo, X.; Small, J. P.; Klare, J. E.; Wang, Y.; Purewal, M. S.; Tam, I. W.; Hong, B. H.; Caldwell, R.; Huang, L.; O'Brien, S.; Yan, J.; Breslow, R.; Wind, S. J.; Hone, J.; Kim, P.; Nuckolls, C. Covalently Bridging Gaps in Single-Walled Carbon Nanotubes with Conducting Molecules. *Science* **2006**, *311*, 356−359.
(3) Choi, S. H.; Kim, B.; Frisbie, C. D. Electrical Resistance of Long Conjugated Molecular Wires. *Science* **2008**, *320*, 1482−1486.
(4) Nijhuis, C. A.; Reus, W. F.; Whitesides, G. M. Molecular Rectification in Metal-SAM-Metal Oxide-Metal Junctions. *J. Am. Chem. Soc.* **2009**, *131*, 17814−17827.
(5) Yan, H.; Bergren, A. J.; Mccreery, R. L.; Della Rocca, M. L.; Martin, P.; Lafarge, P.; Lacroix, J.-C. Activationless Charge Transport across 4.5 to 22nm in Molecular Electronic Junctions. *Proc. Natl. Acad. Sci. U. S. A.* **2013**, *110*, 5326−5330.
(6) Amdursky, N.; Marchak, D.; Sepunaru, L.; Pecht, I.; Sheves, M.; Cahen, D. Electronic Transport via Proteins. *Adv. Mater.* **2014**, *26*, 7142−7161.
(7) Vazquez, H.; Skouta, R.; Schneebeli, S.; Kamenetska, M.; Breslow, R.; Venkataraman, L.; Hybertsen, M. S. Probing the Conductance Superposition Law in Single-Molecule Circuits with Parallel Paths. *Nat. Nanotechnol.* **2012**, *7*, 663−667.
(8) Li, L.; Lo, W.; Cai, Z.; Zhang, N.; Yu, L. Proton-Triggered Switch Based on a Molecular Transistor with Edge-on Gate. *Chem. Sci.* **2016**, *7*, 3137−3141.
(9) Xiang, L.; Palma, J. L.; Bruot, C.; Mujica, V.; Ratner, M. A.; Tao, N. J. Intermediate Tunnelling−hopping Regime in DNA Charge Transport. *Nat. Chem.* **2015**, *7*, 221−226.
(10) Su, T. A.; Neupane, M.; Steigerwald, M. L.; Venkataraman, L.; Nuckolls, C. Chemical Principles of Single-Molecule Electronics. *Nat. Rev. Mater.* **2016**, *1*, 16002.
(11) Dell, E. J.; Capozzi, B.; Xia, J.; Venkataraman, L.; Campos, L. M. Molecular Length Dictates the Nature of Charge Carriers in Single-Molecule Junctions of Oxidized Oligothiophenes. *Nat. Chem.* **2015**, *7*, 209−214.
(12) Salomon, A.; Boecking, T.; Chan, C. K.; Amy, F.; Girshevitz, O.; Cahen, D.; Kahn, A. How Do Electronic Carriers Cross Si-Bound Alkyl Monolayers? *Phys. Rev. Lett.* **2005**, *95*, 266807.
(13) Salomon, A.; Boecking, T.; Seitz, O.; Markus, T.; Amy, F.; Chan, C.; Zhao, W.; Cahen, D.; Kahn, A. What Is the Barrier for Tunneling Through Alkyl Monolayers? Results from n- and p-Si−Alkyl/Hg Junctions. *Adv. Mater.* **2007**, *19*, 445−450.
(14) Salomon, A.; Böcking, T.; Gooding, J. J.; Cahen, D. How Important Is the Interfacial Chemical Bond for Electron Transport through Alkyl Chain Monolayers? *Nano Lett.* **2006**, *6*, 2873−2876.
(15) Cohen, R.; Stokbro, K.; Martin, J. M. L.; Ratner, M. A. Charge Transport in Conjugated Aromatic Molecular Junctions: Molecular Conjugation and Molecule-Electrode Coupling. *J. Phys. Chem. C* **2007**, *111*, 14893−14902.
(16) Nitzan, A. Electron Transmission Through Molecules and Molecular Interfaces. *Annu. Rev. Phys. Chem.* **2001**, *52*, 681−750.
(17) Rodriguez-Gonzalez, S.; Xie, Z.; Galangau, O.; Selvanathan, P.; Norel, L.; Van Dyck, C.; Costuas, K.; Frisbie, C. D.; Rigaut, S.; Cornil, J. HOMO Level Pinning in Molecular Junctions: Joint Theoretical and Experimental Evidence. *J. Phys. Chem. Lett.* **2018**, *9*, 2394−2403.
(18) Sayed, S. Y.; Fereiro, J. A.; Yan, H.; McCreery, R. L.; Bergren, A. J. Charge Transport in Molecular Electronic Junctions: Compression of the Molecular Tunnel Barrier in the Strong Coupling Regime. *Proc. Natl. Acad. Sci. U. S. A.* **2012**, *109*, 11498−11503.
(19) Van Dyck, C.; Geskin, V.; Cornil, J. Fermi Level Pinning and Orbital Polarization Effects in Molecular Junctions: The Role of Metal Induced Gap States. *Adv. Funct. Mater.* **2014**, *24*, 6154−6165.
(20) Xie, Z.; Bâldea, I.; Oram, S.; Smith, C. E.; Frisbie, C. D. Effect of Heteroatom Substitution on Transport in Alkane Dithiol-Based Molecular Tunnel Junctions: Evidence for Universal Behavior. *ACS Nano* **2017**, *11*, 569−578.
(21) Batra, A.; Darancet, P.; Chen, Q.; Meisner, J. S.; Widawsky, J. R.; Neaton, J. B.; Nuckolls, C.; Venkataraman, L. Tuning Rectification in Single-Molecular Diodes. *Nano Lett.* **2013**, *13*, 6233−6237.
(22) Sangtarash, S.; Vezzoli, A.; Sadeghi, H.; Ferri, N.; O'Brien, H. M.; Grace, I.; Bouffier, L.; Higgins, S. J.; Nichols, R. J.; Lambert, C. J. Gateway State-Mediated, Long-Range Tunnelling in Molecular Wires. *Nanoscale* **2018**, *10*, 3060−3067.
(23) Wierzbinski, E.; Yin, X.; Werling, K.; Waldeck, D. H. The Effect of Oxygen Heteroatoms on the Single Molecule Conductance of Saturated Chains. *J. Phys. Chem. B* **2013**, *117*, 4431−4441.
(24) Zhang, Y.; Soni, S.; Krijger, T. L.; Gordiichuk, P.; Qiu, X.; Ye, G.; Jonkman, H. T.; Herrmann, A.; Zojer, K.; Zojer, E.; Chiechi, R. C. Tunneling Probability Increases with Distance in Junctions Comprising Self-Assembled Monolayers of Oligothiophenes. *J. Am. Chem. Soc.* **2018**, *140*, 15048−15055.
(25) Xu, B.; Xiao, X.; Tao, N. J. Measurements of Single-Molecule Electromechanical Properties. *J. Am. Chem. Soc.* **2003**, *125*, 16164−16165.
(26) Haiss, W.; Wang, C.; Grace, I.; Batsanov, A. S.; Schiffrin, D. J.; Higgins, S. J.; Bryce, M. R.; Lambert, C. J.; Nichols, R. J. Precision Control of Single-Molecule Electrical Junctions. *Nat. Mater.* **2006**, *5*, 995−1002.
(27) Quek, S. Y.; Kamenetska, M.; Steigerwald, M. L.; Choi, H. J.; Louie, S. G.; Hybertsen, M. S.; Neaton, J. B.; Venkataraman, L. Mechanically Controlled Binary Conductance Switching of a Single-Molecule Junction. *Nat. Nanotechnol.* **2009**, *4*, 230−234.
(28) Diez-Perez, I.; Hihath, J.; Hines, T.; Wang, Z.-S.; Zhou, G.; Müllen, K.; Tao, N. Controlling Single-Molecule Conductance

through Lateral Coupling of π Orbitals. *Nat. Nanotechnol.* **2011**, *6*, 226−231.
(29) Bruot, C.; Hihath, J.; Tao, N. Mechanically Controlled Molecular Orbital Alignment in Single Molecule Junctions. *Nat. Nanotechnol.* **2012**, *7*, 35−40.
(30) Frisenda, R.; Janssen, V. A. E. C.; Grozema, F. C.; van der Zant, H. S. J.; Renaud, N. Mechanically Controlled Quantum Interference in Individual π-Stacked Dimers. *Nat. Chem.* **2016**, *8*, 1099−1104.
(31) Li, Y.; Haworth, N. L.; Xiang, L.; Ciampi, S.; Coote, M. L.; Tao, N. Mechanical Stretching-Induced Electron-Transfer Reactions and Conductance Switching in Single Molecules. *J. Am. Chem. Soc.* **2017**, *139*, 14699−14706.
(32) Xie, Z.; Bâldea, I.; Demissie, A. T.; Smith, C. E.; Wu, Y.; Haugstad, G.; Frisbie, C. D. Exceptionally Small Statistical Variations in the Transport Properties of Metal−Molecule−Metal Junctions Composed of 80 Oligophenylene Dithiol Molecules. *J. Am. Chem. Soc.* **2017**, *139*, 5696−5699.
(33) Kokalj, A. Computer Graphics and Graphical User Interfaces as Tools in Simulations of Matter at the Atomic Acale. *Comput. Mater. Sci.* **2003**, *28*, 155−168.
(34) Frisch, M. J.; Trucks, G. W.; Schlegel, H. B.; Scuseria, G. E.; Robb, M. A.; Cheeseman, J. R.; Scalmani, G.; Barone, V.; Mennucci, B.; Petersson, G. A.; Nakatsuji, H.; Caricato, M.; Li, X.; Hratchian, H. P.; Izmaylov, A. F.; Bloino, J.; Zheng, G.; Sonnenberg, J. L.; Hada, M.; Ehara, M.; Toyota, K.; Fukuda, R.; Hasegawa, J.; Ishida, M.; Nakajima, T.; Honda, Y.; Kitao, O.; Nakai, H.; Vreven, T.; Montgomery, J. A.; Peralta, J. E., Jr; Ogliaro, F.; Bearpark, M.; Heyd, J. J.; Brothers, E.; Kudin, K. N.; Staroverov, V. N.; Keith, T.; Kobayashi, R.; Normand, J.; Raghavachari, K.; Rendell, A.; Burant, J. C.; Iyengar, S. S.; Tomasi, J.; Cossi, M.; Rega, N.; Millam, J. M.; Klene, M.; Knox, J. E.; Cross, J. B.; Bakken, V.; Adamo, C.; Jaramillo, J.; Gomperts, R.; Stratmann, R. E.; Yazyev, O.; Austin, A. J.; Cammi, R.; Pomelli, C.; Ochterski, J. W.; Martin, R. L.; Morokuma, K.; Zakrzewski, V. G.; Voth, G. A.; Salvador, P.; Dannenberg, J. J.; Dapprich, S.; Daniels, A. D.; Farkas, O.; Foresman, J. B.; Ortiz, J. V.; Cioslowski, J.; Fox, D. J. *Gaussian 09*, Revision B.01; Gaussian, Inc.: Wallingford, CT, 2010.
(35) Allouche, A. Software News and Updates Gabedit — A Graphical User Interface for Computational Chemistry Softwares. *J. Comput. Chem.* **2011**, *32*, 174−182.
(36) Stanton, J. F.; Gauss, J.; Harding, M. E.; Szalay, P. G.; Auer, A. A.; Bartlett, R. J.; Benedikt, U.; Berger, C.; Bernholdt, D. E.; Bomble, Y. J.; Cheng, L.; Christiansen, O.; Heckert, M.; Helgaker, T.; Heun, O.; Huber, C.; Jagau, T.-C.; Jensen, H. J. A.; Jonsson, D.; Jørgensen, P.; Jusélius, J.; Klein, K.; Lauderdale, W. J.; Matthews, D. A.; Metzroth, T.; Mitin, A. V.; Mück, L. A.; Olsen, J.; O'Neill, D. P.; Price, D. R.; Prochnow, E.; Puzzarini, C.; Ruud, K.; Schiffmann, F.; Schwalbach, W.; Simmons, C.; Stopkowicz, S.; Tajti, A.; Taylor, P. R.; Vázquez, J.; Wang, F.; Watts, J. D. *CFOUR, Coupled-Cluster Techniques for Computational Chemistry: A Quantum-Chemical Program Package*; 2010.
(37) Bâldea, I. A Quantum Chemical Study from a Molecular Transport Perspective: Ionization and Electron Attachment Energies for Species Often Used to Fabricate Single-Molecule Junctions. *Faraday Discuss.* **2014**, *174*, 37−56.
(38) Love, J. C.; Estroff, L. A.; Kriebel, J. K.; Nuzzo, R. G.; Whitesides, G. M. Self-Assembled Monolayers of Thiolates on Metals as a Form of Nanotechnology. *Chem. Rev.* **2005**, *105*, 1103−1169.
(39) Laibinis, P. E.; Whitesides, G. M.; Allara, D. L.; Tao, Y.-T.; Parikh, A. N.; Nuzzo, R. G. Comparison of the Structures and Wetting Properties of Self-Assembled Monolayers of n-Alkanethiols on the Coinage Metal Surface, Cu, Ag, Au. *J. Am. Chem. Soc.* **1991**, *113*, 7152−7167.
(40) Haugstad, G. *Atomic Force Microscopy*; John Wiley & Sons: Hoboken, NJ, 2012.
(41) Demissie, A. T.; Haugstad, G.; Frisbie, C. D. Quantitative Surface Coverage Measurements of Self-Assembled Monolayers by Nuclear Reaction Analysis of Carbon-12. *J. Phys. Chem. Lett.* **2016**, *7*, 3477−3481.
(42) Engelkes, V. B.; Beebe, J. M.; Frisbie, C. D. Length-Dependent Transport in Molecular Junctions Based on SAMs of Alkanethiols and Alkanedithiols: Effect of Metal Work Function and Applied Bias on Tunneling Efficiency and Contact Resistance. *J. Am. Chem. Soc.* **2004**, *126*, 14287−14296.
(43) Xie, Z.; Bâldea, I.; Frisbie, C. D. Why One Can Expect Large Rectification in Molecular Junctions Based on Alkane Monothiols and Why Rectification Is So Modest. *Chem. Sci.* **2018**, *9*, 4456−4467.
(44) Li, C.; Pobelov, I.; Wandlowski, T.; Bagrets, A.; Arnold, A.; Evers, F. Charge Transport in Single Au | Alkanedithiol | Au Junctions: Coordination Geometries and Conformational Degrees of Freedom. *J. Am. Chem. Soc.* **2008**, *130*, 318−326.
(45) Song, H.; Kim, Y.; Jang, Y. H.; Jeong, H.; Reed, M. A.; Lee, T. Observation of Molecular Orbital Gating. *Nature* **2009**, *462*, 1039−1043.
(46) Alloway, D. M.; Hofmann, M.; Smith, D. L.; Gruhn, N. E.; Graham, A. L.; Colorado, R.; Wysocki, V. H.; Lee, T. R.; Lee, P. A.; Armstrong, N. R. Interface Dipoles Arising from Self-Assembled Monolayers on Gold: UV - Photoemission Studies of Alkanethiols and Partially Fluorinated Alkanethiols. *J. Phys. Chem. B* **2003**, *107*, 11690−11699.
(47) Qi, Y.; Yaffe, O.; Tirosh, E.; Vilan, A.; Cahen, D.; Kahn, A. Filled and Empty States of Alkanethiol Monolayer on Au (111): Fermi Level Asymmetry and Implications for Electron Transport. *Chem. Phys. Lett.* **2011**, *511*, 344−347.
(48) Bâldea, I. Ambipolar Transition Voltage Spectroscopy: Analytical Results and Experimental Agreement. *Phys. Rev. B: Condens. Matter Mater. Phys.* **2012**, *85*, No. 035442.
(49) Xie, Z.; Bâldea, I.; Smith, C. E.; Wu, Y.; Frisbie, C. D. Experimental and Theoretical Analysis of Nanotransport in Oligophenylene Dithiol Junctions as a Function of Molecular Length and Contact Work Function. *ACS Nano* **2015**, *9*, 8022−8036.
(50) Beebe, J. M.; Kim, B.; Gadzuk, J. W.; Frisbie, C. D.; Kushmerick, J. G. Transition from Direct Tunneling to Field Emission in Metal-Molecule-Metal Junctions. *Phys. Rev. Lett.* **2006**, *97*, No. 026801.
(51) Haug, H. J. W.; Jauho, A.-P. *Quantum Kinetics in Transport and Optics of Semiconductors*, 2nd ed.; Springer Series in Solid-State Sciences: Berlin, 2008; Vol. *123*.
(52) Goddard, R.; Haenel, M. W.; Krüger, C.; Herndon, W. C.; Zander, M. Crystallization of Large Planar Polycyclic Aromatic Hydrocarbons: The Molecular and Crystal Structures of Hexabenzo-[Bc,Ef,Hi,Kl,No,Qr]Coronene and Benzo[1,2,3-Bc:4,5,6-b'c']-Dicoronene. *J. Am. Chem. Soc.* **1995**, *117*, 30−41.
(53) Li, X. C.; Sirringhaus, H.; Garnier, F.; Holmes, A. B.; Moratti, S. C.; Feeder, N.; Clegg, W.; Teat, S. J.; Friend, R. H. A Highly π-Stacked Organic Semiconductor for Thin Film Transistors Based on Fused Thiophenes. *J. Am. Chem. Soc.* **1998**, *120*, 2206−2207.
(54) Brédas, J.-L.; Calbert, J. P.; Filho, D. A. da S.; Cornil, J. Organic Semiconductors: A Theoretical Characterization of the Basic Parameters Governing Charge Transport. *Proc. Natl. Acad. Sci. U. S. A.* **2002**, *99*, 5804−5809.
(55) McGarry, K. A.; Xie, W.; Sutton, C.; Risko, C.; Wu, Y.; Young, V. G.; Brédas, J. L.; Frisbie, C. D.; Douglas, C. J. Rubrene-Based Single-Crystal Organic Semiconductors: Synthesis, Electronic Structure, and Charge-Transport Properties. *Chem. Mater.* **2013**, *25*, 2254−2263.
(56) Bâldea, I. A Surprising Way to Control the Charge Transport in Molecular Electronics: The Subtle Impact of the Coverage of Self-Assembled Monolayers of Floppy Molecules Adsorbed on Metallic Electrodes. *Faraday Discuss.* **2017**, *204*, 35−52.
(57) Bâldea, I. A Sui Generis Electrode-Driven Spatial Confinement Effect Responsible for Strong Twisting Enhancement of Floppy Molecules in Closely Packed Self-Assembled Monolayers. *Phys. Chem. Chem. Phys.* **2018**, *20*, 23492−23499.

DOI: 10.1021/jacs.8b11248
J. Am. Chem. Soc. 2019, 141, 497−504